Effect of electrical coupling on ionic current and synaptic potential measurements

Pascale Rabbah[(2)], **Jorge Golowasch**[(1,2)], **Farzan Nadim**[(1,2)]

[(1)] Department of Mathematical Sciences and
Center for Applied Mathematics and Statistics
New Jersey Institute of Technology, Newark, NJ 07102

[(2)] Dept of Biological Sciences, Rutgers University-Newark

CAMS Report 0405-08, Fall 2004

Center for Applied Mathematics and Statistics

NJIT

Effect of electrical coupling on ionic current and synaptic potential measurements

Pascale Rabbah[1], Jorge Golowasch[1,2] and Farzan Nadim[1,2]

[1]Department of Biological Sciences, Rutgers University, Newark, NJ 07102

[2]Department of Mathematical Sciences, New Jersey Institute of Technology, Newark, NJ 07102

Running head: Electrical coupling effects on voltage clamp measurements

Contact Information:

Jorge Golowasch, Dept. of Biological Sciences, 101 Warren St., Newark, NJ 07102.

Phone: 973-353-1267, Fax: 973-353-1007. Email: Jorge.P.Golowasch@njit.edu

Abstract

Recent studies have found electrical coupling to be more ubiquitous than previously thought, and coupling through gap junctions is known to play a crucial role in neuronal function and network output. In particular, current spread through gap junctions may affect the activation of voltage-dependent conductances as well as chemical synaptic release. Using voltage-clamp recordings of two strongly electrically coupled neurons of the lobster stomatogastric ganglion and conductance-based models of these neurons, we identified effects of electrical coupling on the measurement of leak and voltage-gated outward currents, as well as synaptic potentials. Experimental measurements showed that both leak and voltage-gated outward currents are recruited via gap junctions from neurons coupled to the clamped cell. Nevertheless, in spite of the strong coupling between these neurons (~23%), the errors made in estimating voltage-gated conductance parameters were relatively minor (<10%). Thus, in many cases isolation of coupled neurons may not be required if a small degree of measurement error of the voltage-gated currents or the synaptic potentials is acceptable. Modeling results show, however, that such errors may be as high as 20% if the gap junction position is near the recording site or as high as 90% when measuring smaller voltage-gated ionic currents. Paradoxically, improved space clamp increases the errors due to electrical coupling because voltage control across gap junctions is poor for even the highest realistic coupling conductances. Furthermore, the common procedure of leak subtraction can add an extra error to the conductance measurement, the sign of which depends on the maximal conductance.

Keywords: Electrotonic, voltage clamp, stomatogastric, leak current, modeling, gap junction

Introduction

Gap junctions have high permeability to ions and small molecules. The flow of small molecules across a gap junction is a process that affects concentrations in both coupled cells locally. This diffusional effect is known to determine the spread of Ca^{++} waves through astrocytes (Rose and Konnerth 2001) and neurons (Kandler and Katz 1998), crossing of metabolites such as Ca^{++} (Saez et al. 1989), IP3 (Kandler and Katz 1998; Rose and Konnerth 2001) and cAMP, (Kam et al. 1998; Saez et al. 1989), and in other processes such as carcinogenesis (Mesnil 2002; Trosko and Chang 2001) and embryogenesis (Bauer et al. 2004; Kandler and Katz 1998; Sullivan et al. 1998). By contrast, electric currents crossing gap junctions spread over long distances, and can affect electric processes throughout the coupled neurons. The physiological consequences of this electrical coupling include synchronization of electrical activity (Bennett and Zukin 2004; Komendantov and Canavier 2002; Pfeuty et al. 2003; Saint-Amant and Drapeau 2001), prolongation of epileptiform discharges (Perez-Velazquez et al. 1994), coordination of certain motor behavior (Moore and Grace 2002), coincidence detection (Edwards et al. 1998) and motor-pattern generation (Traub et al. 1999; Tresch and Kiehn 2000; Whittington and Traub 2003).

Electrical coupling can dramatically change the activity of neurons in a network. Thus, understanding the contribution of gap junctions to network function requires relatively accurate measurements of the ionic conductances expressed by the neurons involved. There have been some experimental (Rorig et al. 1996) and theoretical studies (Poznanski 1999; Veenstra 2001) analyzing the contribution of electrotonic coupling to electrical current spread between neurons and other cell types. However, due to the

scarcity of specific pharmacological gap junction blockers (Bennett and Zukin 2004) and of appropriate biological preparations, estimating the effects of electrical coupling on measurements of ionic currents in neurons presents a difficult problem that needs to be rigorously studied. This issue has acquired further importance due to recent studies that show the presence of electrical coupling in an increasing number of cell types (Bennett and Zukin 2004; Pfeuty et al. 2003; Vandecasteele et al. 2005).

Electrical coupling to other cells can, in principle, produce an increase in either the passive leak or active voltage clamp currents measured from a neuron. The relative contribution in passive or active currents from one cell to its gap junctional neighbor also depends on the leakiness of both, including the effects of electrode impalement on input resistance, as this will affect their electrotonic compactness. Pharmacological agents that block gap junctions are well known for their frequent lack of specificity (Bennett and Zukin 2004), and photoinactivation causes the release of cellular contents and free radicals that can damage or affect neighboring cells (Dahle et al. 2001). Consequently, the convenience of removing synaptic neighbors either pharmacologically or by photoinactivation (Dahle et al. 2001; Miller and Selverston 1979) when attempting to measure ionic currents or membrane potential changes is not assured. Therefore, when doing voltage clamp measurements from gap-junctionally coupled neurons, it would be useful to have appropriate criteria to determine when to choose between cell isolation versus accepting measurement errors produced by electrical coupling.

In this study, we used electrophysiology and conductance-based models to examine the effect of electrical coupling on the measurements of passive and voltage-gated potassium currents as well as elicited postsynaptic potentials. As a model system,

we used somatic recordings of the two pyloric dilator (PD) neurons and the postsynaptic lateral pyloric (LP) neuron in the lobster stomatogastric ganglion (STG), as well as computational models of this network. The two PD neurons are strongly electrically coupled and are believed to be structurally and functionally identical. The PD neurons exhibit identical intrinsic properties, make and receive identical synapses and, as members of the pyloric pacemaker group, always oscillate in synchrony (Ayali and Harris-Warrick 1999; Eisen and Marder 1984; Hooper 1997; Miller and Selverston 1982). We compared the total, leak and leak-subtracted currents, as well as synaptic potentials, measured when the two PD neurons were functionally uncoupled by voltage clamping both somata to the same membrane potential and when only one PD neuron soma was voltage clamped. This comparison provided a measure of the distortion that a gap-junctionally coupled neuron produces in voltage clamp measurements of ionic currents.

METHODS

Experimental setup

Experiments were conducted on adult male spiny lobsters (*Panulirus interruptus*), weighing 400-800 gm. Animals were purchased from Don Tomlinson Fisheries (San Diego, CA) and were kept in artificial seawater tanks at 12-15^{0}C until use. The animals were anesthetized by packing on ice for 30 minutes prior to the dissection. The stomatogastric nervous system (STNS; including the STG, the esophageal and the paired commissural ganglia) was isolated using standard methods (Harris-Warrick 1992; Selverston et al. 1976). The STNS was pinned down in a Sylgard-coated Petri dish and the STG was desheathed to allow penetration of the cell bodies and effective superfusion of the neurons. The preparations were superfused with normal saline at 18^{0}C, pH 7.35, containing (in mM): 12.8 KCl, 479 NaCl, 13.7 $CaCl_2$, 10.0 $MgSO_4$, 3.9 $NaSO_4$, 11.2 Trizma base, and 5.1 Maleic acid. For neuron impalement, microelectrodes were pulled using a Flaming-Brown micropipette puller (P87, Sutter Instruments, CA) and filled with 3 M KCl to give resistances of 8-13 MΩ. Identification of the neurons was accomplished by matching intracellular action potential recordings to their corresponding extracellular recordings on motor nerves (Harris-Warrick 1992; Selverston et al. 1976). After identification, the neurons were impaled with two electrodes each and the preparation was superfused with 10^{-7} M Tetrodotoxin (TTX; Biotium, Hayward, CA) in order to block sodium inward currents and hence action potentials. Slow rhythmic activity is also blocked in TTX (Raper 1979).

Using the two-electrode voltage clamp method, either one (1VC) or both (2VC) PD neurons were voltage clamped using Axoclamp 2B amplifiers (Axon Instruments, Union City, CA). For the 1VC protocol, one PD neuron was voltage clamped to a holding potential of −40 mV (to remove the contribution of the large transient A current (Harris-Warrick et al. 1995)) while the other PD neuron was recorded in current clamp. A 2 sec, 10 mV hyperpolarizing pulse followed by 2 second depolarizing pulses ranging in amplitude from 5 to 60 mV were applied to the voltage-clamped PD neuron. The initial hyperpolarizing pulse was used to determine the leak current and, when necessary, to leak subtract the depolarization-induced currents after appropriately scaling it. For the 2VC protocol, both PD neurons were always voltage clamped to the same membrane voltage. Assuming identical electrotonic structure of the two electrically coupled neurons, this protocol would effectively uncouple the neurons due to the fact that the gap-junctional current is proportional to the difference between the membrane potentials of the two neurons. All depolarizing pulses elicited a total current I_{total} that consisted largely of potassium outward currents I_K and passive leak current I_{leak}. An inward Ca^{++} current is also included in this total current but its amplitude is negligible (<1%) compared to I_K + I_{leak} (Golowasch and Marder 1992; Graubard and Hartline 1991; Johnson et al. 2003).

Both PD neurons also establish inhibitory cholinergic synaptic connections to multiple follower neurons, including the LP neuron (Eisen and Marder 1982). These synapses show voltage-dependent (graded) release of neurotransmitter. In order to measure the graded component of the PD to LP synapse, each PD neuron was impaled with two electrodes and the LP neuron was impaled with a single electrode in saline containing 10^{-7} M TTX to block rhythmic activity and action potential-mediated synaptic

transmission (Raper 1979). To study the effect of electrical coupling on PD to LP synaptic release, either PD_1 (1VC protocol) or both PD_1 and PD_2 (2VC protocol) were voltage clamped at −60 mV while LP (and PD_2 in 1VC only) was recorded in current clamp. A series of 2 second depolarizing pulses to voltages ranging from −50 to −10 mV was applied to the voltage clamped PD neuron(s) to activate the PD to LP synapse. The LP resting membrane potential was set to −50 mV by current injection so that the inhibitory postsynaptic potentials (IPSPs) which had typical amplitudes of 1-7 mV (depending on the presynaptic membrane potential) did not saturate the membrane potential at the synaptic reversal potential of −85 to −80 mV (Eisen and Marder 1982).

An NI PCI-6070-E board (National Instruments, Austin, TX) was utilized for data acquisition and for current injection with the data acquisition software Scope (available for download at http://stg.rutgers.edu/software) developed in the LabWindows/CVI software environment (National Instruments, Austin, TX) on a Windows operating system. The acquired data were then saved as individual binary and ASCII files and were analyzed on a Linux platform. Statistica (Statsoft, Tulsa, OK) and Origin (OriginLab, Natick, MA) software packages were used for statistical and graphical analysis. Reported statistical significance indicates that the achieved significance level *P* was below the critical significance level α=0.05. All error bars shown denote standard deviation.

Model

Integrations of membrane and cable equations were performed using Network, a home-developed software running on the Linux platform, using a 4^{th} order Runge-Kutta

method with a time step of 5 μs. In our *standard model*, two somata of 180 μm diameter connected to respective multi-compartment cylindrical cables 500 μm long and 20 μm in diameter were coupled with a gap junction of conductance $g_c = 10^{-6}$ S between the last segment of each cable. The model neuron is representative of the biological PD neuron, which is a monopolar neuron with a large soma coupled to a relatively large primary neurite (King 1976a, b). In this study we ignored the effects of the secondary and tertiary neurites. Each cable was divided into five 100 μm long compartments and both have geometry-independent specific membrane resistivity $R_m = 40000\ \Omega\text{cm}^2$ (corresponding to a leak conductance of $G_m = 0.025\ \text{mS/cm}^2$), specific axial resistivity $R_i = 60\ \Omega\text{cm}$, and specific membrane capacitance $C_m = 10^{-6}\ \text{F/cm}^2$ (Hartline and Castelfranco 2003). Each neuron was modeled as a "Rall neuron" by combining the soma with the first segment of the cable (Johnston and Wu 1995; Rall et al. 1995). The length of the model neurons or the position of the gap junctions were varied as stated in the Results.

Both PD model neurons were identical and contained a homogeneously distributed leak current with $E_{leak} = -50$ mV and both slow (KS) and fast (KF) inactivating outward potassium currents characterized by:

$$i_K = [\bar{g}_{KS} m_S h_S + \bar{g}_{KF} {m_F}^3 h_F](V_{PD} + 80)$$

$$10\frac{dm_S}{dt} = (m_{S\infty} - m_S) \qquad m_{S\infty} = \frac{1}{1+e^{-(V_m+4)/6}}$$

$$\tau_{hS}\frac{dh_S}{dt} = (h_{S\infty} - h_S) \qquad h_{S\infty} = \frac{1}{1+e^{(V_m+52)/28}}$$

$$\tau_{hS} = 2000 + \frac{2200}{1+e^{-(V_m-7)/25}}$$

$$8\frac{dm_F}{dt} = (m_{F\infty} - m_F) \qquad m_{F\infty} = \frac{1}{1+e^{-(V_m+10)/5}}$$

$$70\frac{dh_F}{dt} = (h_{F\infty} - h_F) \qquad h_{F\infty} = \frac{1}{1+e^{(V_m+38)/5}}$$

with $\bar{g}_{KS}$ = 5 mS/cm^2, $\bar{g}_{KF}$ = 1.4 mS/cm^3. Gap junctional coupling between the two PD neurons was modeled by adding a symmetric coupling current term to the coupled compartments of each cell:

$$i_{C(PD1)} = g_C(V_{PD2} - V_{PD1})$$
$$i_{C(PD2)} = g_C(V_{PD1} - V_{PD2})$$

The LP neuron received identical synaptic input from each PD neuron (except when stated) and the synaptic current was described by:

$$i_{syn(PDx)} = (g_{synT} h_{syn} + g_{synP}) m_{syn} (V_{LP} - E_{syn})$$

$$75\frac{dm_{syn}}{dt} = m_{syn\infty} - m_{syn} \qquad m_{syn\infty} = \frac{1}{1+e^{-(V_{PDx}+25)/12}}$$

$$500\frac{dh_{syn}}{dt} = h_{syn\infty} - h_{syn} \qquad h_{syn\infty} = \frac{1}{1+e^{(V_{PDx}+35)/6}}$$

where g_{synT} = 5 μS/cm^2 and g_{synP} = 2 μS/cm^2. The LP neuron was modeled as a single compartment spherical cell 125 μm in diameter with the following properties:

$$C_{m(LP)}\frac{dV_{LP}}{dt} = -\frac{1}{R_m}(V_{LP} + 40) - i_{syn(PD1)} - i_{syn(PD2)}$$

with $C_{m(LP)} = 10^{-6}$ F/cm^2 and $R_m = 25000$ Ωcm^2.

The 1VC protocol was modeled by clamping the voltage of the PD_1 neuron soma and recording the total current. The 2VC protocol was modeled by clamping the soma of PD_1 and PD_2 to the same voltage and recording the total current from PD_1 (identical results are obtained if g_C is set to zero and the 1VC protocol is applied). Leak subtraction was performed exactly as described for the biological current measurements.

RESULTS

The two PD neurons are strongly electrically coupled via gap junctions and always show synchronous membrane potential oscillations interrupted by unitary IPSPs from the LP neuron (Fig. 1A). Both PD neurons also synaptically inhibit the LP neuron but the synapse is too slow to show individual spike-mediated IPSPs (Fig. 1B, thick traces). To investigate the effect of electrical coupling on ionic current measurements, both PD_1 and PD_2 neurons were impaled with two electrodes and voltage clamped at a holding potential of –40mV (Fig. 1B; 2VC protocol, see Methods). Figure 1B shows the leak current measured in response to a voltage step to –50 mV (thin traces) and outward currents measured in response to a voltage step to 0 mV (thick traces). As seen in this figure, the outward currents measured from the two PD neurons were always nearly identical. The bottom trace shows the IPSP in the LP neuron in response to the depolarizing voltage step in the PD neurons.

The effect of electrical coupling on passive ionic current measurements

All depolarizing pulses elicited a total current I_{total} that consisted mainly of potassium outward currents I_K and passive leak current I_{leak} (see Methods). When only one PD neuron was voltage clamped (1VC protocol) and stepped to different voltage levels, the membrane potential of the second PD neuron was also affected (see, for example, thick V_{PD_2} trace in Fig. 2A). Due to the fact that V_{PD_1} and V_{PD_2} were not identical in the 1VC protocol, PD_2 contributed an additional current to the measurement of the total current from the PD_1 soma. This was the current that flowed through the gap

junction between the two neurons. However, when both PD neurons were clamped to the same voltage (assuming they had identical electrotonic characteristics), this gap junction current was eliminated. A greater I_{leak} for 1VC (coupled) as compared to 2VC (uncoupled) was therefore expected. Figure 2A shows a 10 mV hyperpolarizing step in the voltage clamped PD neuron(s) and the (leak) current recorded. I_{leak} for the coupled neurons (1VC, thick traces) was greater than I_{leak} for the uncoupled neurons (2VC, thin traces). When only one neuron was voltage clamped (1VC), the second neuron (Fig 2A, middle panel, thick trace) showed an attenuated change in voltage. The apparent coupling ratio ($\Delta V_{post}/\Delta V_{pre}$) determined using hyperpolarizing pulses was 0.232 ± 0.062 (N = 9). The leak conductance, calculated as the ratio $I_{leak}/\Delta V_{hyp}$, was significantly larger in PD_1 for 1VC, measuring 0.238 ± 0.144 μS, than in 2VC, which measured 0.193 ± 0.109 μS (Fig. 2B; Student's *t*-test, $P = 0.00846$; N = 12). This corresponds to approximately a 23% overestimate of the leak conductance of the isolated (uncoupled) PD neuron.

The effect of electrical coupling on voltage-gated current measurements

The flow of current across the gap junction when only one PD neuron is voltage clamped could, in principle, activate voltage-gated currents in the unclamped partner as well as in the clamped neuron. As in the case of the leak current measurement, we measured a greater total current with the 1VC protocol (coupled neurons) than when both cells were uncoupled with the 2VC protocol (Fig. 3A). This difference was present in both the total (Fig. 3A and B, top panels) and the leak-subtracted (not shown) currents, indicating that the voltage step in PD_1 with the 1VC protocol resulted in activation of

voltage-gated currents in PD_2 and not simply a recruitment of leak current from the unclamped neuron. The difference between currents measured in the 1VC and 2VC conditions was observed at all voltage clamp steps above −25mV (two-way ANOVA, $P = 0.0107$ for peak currents and $P = 0.0083$ for steady state currents, N = 12). The 1VC leak subtracted currents were also significantly larger than the 2VC measured currents at all voltages above −25mV, ($P = 0.0179$ for peak, $P = 0.001$ for steady state, N = 12; not shown). High-threshold K^+ currents are known to activate at –25mV and higher in these neurons (Golowasch and Marder 1992; Graubard and Hartline 1991; Harris-Warrick et al. 1995; Johnson et al. 2003). The peak current was measured between 50-100 ms and the steady state current at the end of the 2 second long voltage step.

The bottom panels of Figures 3A and B show the model equivalent of the voltage clamp results shown in the top panels. The parameters of the model of the two coupled PD neurons (see Methods) were adjusted to fit both 1VC and 2VC results of a single representative experiment (shown in Fig. 3A) not the average data (cf. (Golowasch et al. 2002; Prinz et al. 2004). The model IV curves are shown in Figure 3B. The two PD model neurons were identical and consisted of a soma coupled to a single 500 µm long neurite with the gap junction located between the tips of the neurites (Fig. 1 inset).

To quantify the error in the voltage clamp measurements due to electrical coupling, we calculated the difference between the leak subtracted currents measured in the coupled and uncoupled neurons (Dataset same as that used in Figure 3B, Biological, after leak subtraction) as a percentage of the current in the uncoupled neuron (Fig. 4A). For voltage steps to –30 mV the average difference current was close to 50% of the current measured in the uncoupled neuron. However, with larger voltage steps (and hence

with larger currents activated), the difference current due to the electrical coupling was a smaller percentage of the total current. (For the voltage step to –35 mV, the currents were too small to accurately measure the difference.) The normalized difference shown in Fig 4A for steady state currents is not significantly different from the differences observed for peak leak subtracted currents (not shown).

Surprisingly, the parameters of sigmoidal fits (equation: Gmax / $(1+e^{-k[V+V½]})$) to the steady-state (or peak, not shown) conductance vs. membrane potential curves showed little difference between the 1VC and 2VC measurements in either the midpoint (1VC: V½ = –0.4mV, 2VC: V½ = –0.6mV) or slope values (1VC: k = 0.100mV, 2VC: k = 0.107mV) (Fig. 4B). The more prominent, but still small (<10%), difference was in the maximal conductance (1VC: Gmax = 1.79 µS, 2VC: Gmax = 1.63 µS) (Fig. 4B).

It has been shown that averaged data do not necessarily adequately characterize the properties of individual neurons (Golowasch et al. 2002; Prinz et al. 2004). Our model data were fitted to the measurements of a single experiment (rather than to the average data) representative of the average trend that showed larger current values using the 1VC protocol than the 2VC protocol. However, in a small number of experiments (3 out of 15) the 2VC protocol elicited larger total currents than the 1VC protocol. We attempted to adjust the parameters of our model to obtain a good fit to these data, but did not succeed. Our lack of success may indicate that the simple geometry of our model or the assumption of uniform distribution of channels does not capture all cases. However, it seems to correctly reproduce the global effects of uncoupling neurons connected by gap junctions.

Effect of gap junction position along the neurite

Using the model 2-neuron network, we examined the effect of the position of the gap junction on the total current measured. We varied the position of the gap junction along the neurite of the model neurons in a symmetric fashion and measured the total current in 1VC and 2VC conditions. To elucidate the effect of the distance of the gap junction clearly, we chose a 1000 μm long neurite for these measurements. We observed that when the gap junction was located close to the clamped soma, the total current was larger. With the 1VC protocol (red traces, neurons coupled), the closer the gap junction was to the soma, the closer the voltage across the gap junction was to the clamped voltage (not shown) and thus the total current measured was larger (Fig. 5A, panels *i-iii* and Fig. 5B, open red circles). In contrast, with the 2VC protocol (black traces) the total current was independent of the gap junction position because the two neurons were effectively uncoupled. As the gap junction was moved further away from the soma, the total current under 1VC and 2VC conditions approach each other. However, the total current under 1VC was higher at all positions due to the fact that the neurites were not infinitely long cables. Consequently, the second neuron contributed a fixed, non-zero current even when the gap junction was positioned at the tip of the neurites (Fig. 5B, open circles). Figure 5C (open symbols) shows the percentage of additional current measured in 1VC compared to 2VC (the current difference between 1VC and 2VC normalized to 2VC). The largest difference (~18%) was observed for the gap junction positions closest to the soma, and the difference dropped rapidly as the gap junction was moved away from it (Fig. 5C, open symbols).

We also examined the difference between current measurements in 1VC and 2VC conditions as the length of the neurite was varied but the gap junction position was maintained between the tips of the neurites instead of varying the gap junction position along a neurite of constant length. In this case, the total measured current decreased as the length of the neurite decreased due to the drop in the total cell surface, hence lower total conductance (Fig. 5A, panels *iii*-*v* and Fig. 5B, solid circles). However, similar to the fixed-length case, more current was recruited when only one neuron was clamped and thus both cells were coupled (Fig. 5A, panels *iii*-*v*, red traces, and Fig. 5B solid red circles) than in the 2VC case, when the two neurons were uncoupled (Fig. 5A, panels *iii*-*v*, black traces, and Fig. 5B solid black circles). As the length of the neurites was increased, the total current also increased, converging on the values observed for cables of fixed length but varying gap junction position described above (Fig. 5B). The normalized current difference decreased with increased length as expected for cells that become increasingly less electrotonically compact (Fig. 5C, solid symbols). Compared to the case with fixed length neurites and moving gap junction positions (Fig. 5C, open symbols), the normalized current difference was lower at all neurite lengths, a reflection of the higher electrotonic compactness of shorter cables (Fig. 5C, solid symbols).

Current measurements as a function of leak and K^+ conductances

The electrotonic structure has a crucial influence on how well the voltage of a neuron can be controlled across a gap junction, as demonstrated by the effects of the position of a gap junction along the neurite (and the length of the neurite) described in the

previous section. To understand the effect of changes in electrotonic structure due to membrane resistance on measured currents, we varied both the leak conductance and the maximal conductance of the K^+ current in our standard model. Figure 6A shows the expected increase in total current measured as the leak conductance (G_m) is varied. With increasing leak conductance, the total measured current increased approximately linearly, whether the two neurons are coupled (1VC) or not (2VC; note that the apparent exponential increase is due to the fact that the abscissa has a logarithmic scale). We observed a small difference in total current between coupled and uncoupled conditions (Fig. 6A, inset), with the total current of the coupled neurons always higher. This difference was mostly due to the activation of the K^+ currents in the second neuron (in 1VC, as seen also in Fig. 3). Figure 6B shows the difference between coupled and uncoupled total and leak-subtracted currents as a percentage of the uncoupled current. The difference in the total current (black symbols) was constant at low leak conductance values but decreased monotonically to zero as the leak conductance increased and the gap junction became electrotonically distant from the soma, effectively uncoupling the two neurons.

When the conductance of the K^+ current was changed, we observed an almost identical behavior as when the leak conductance was varied: the total current grew whether the neurons were coupled or not (Fig. 6C; as in panel A, the apparent exponential change here is due to the logarithmic scale of the abscissa). Again, we observed a small difference in total current, with the coupled (1VC) neurons producing more current than the uncoupled (2VC) neurons for all values of the K^+ conductance (Fig. 6C, inset). Similar to when the leak conductance was varied (Fig. 6B, black

symbols), the normalized total current difference decreased monotonically towards zero as the K^+ conductance was increased (Fig. 6D, black circles). This was due to the fact that, as conductance was increased, the gap junction became electrotonically more distant from the soma, effectively uncoupling the neurons.

In contrast with the total current, the leak-subtracted K^+ currents showed a different and somewhat non-intuitive dependence on the conductance of the cells (Fig. 6B & D, red circles). For small values of G_m, the normalized leak-subtracted K^+ current difference was positive, i.e. the leak-subtracted current was larger when the two neurons were coupled than when they were uncoupled (Fig. 6B, red circles). However, for larger G_m values, the K^+ current became smaller when the cells were coupled than when they were uncoupled and the leak-subtracted current difference became negative. As G_m was increased even further, the difference reversed toward zero. This odd behavior can be explained as follows. When the soma of cell 1 is voltage clamped and a positive voltage pulse is applied, the gap-junctionally coupled cell 2 contributes to the current measured from cell 1 soma in two ways. First, the gap junction allows some K^+ channels to be opened in cell 2 thereby adding to the (leak-subtracted) K^+ current measured from the soma of cell 1. Second, cell 2 puts a passive load on cell 1 and dampens the depolarization of the compartments of cell 1 that are near the gap junction. This latter effect is reflected in the fact that the membrane potential of the cell 1 compartment adjacent to the gap junction is lower when cell 1 is coupled to cell 2 than in an isolated cell 1 (not shown). This, in turn, results in less K^+ current activation in cell 1 thereby reducing the K^+ current measured in cell 1, while the leak current measured is still higher because the neurons are electrotonically more compact (less membrane conductance)

during the hyperpolarizing pulse. Thus, the two contributions of cell 2 to the K^+ current measured from cell 1 work in opposition to one another. If the leak conductance is small, the first effect dominates and there is a net increase in K^+ current as measured from the soma of cell 1. In contrast, if the leak conductance is large, the second effect dominates and there is a net decrease in the amount of activated K^+ current and an increase in the measured leak current. The leak subtraction procedure then reduces the net current in the coupled case proportionally more than in the uncoupled case, thus leading to a negative current difference and strong non-linearity of the (normalized) current difference (Fig. 6B, red symbols). The same effect on the electrotonic structure of the neurons occurred when the K^+ conductance was changed and a similar nonlinear phenomenon was observed at high K^+ conductance values, albeit much less pronounced than when the leak conductance was modified (Fig. 6D, red symbols; magnified in the inset).

Effect of gap junction on measuring the synaptic response

The two PD neurons synapse onto the LP neuron and, upon depolarization, produce a graded inhibitory postsynaptic potential in the LP neuron (Fig. 7A inset and schematic inset of Fig. 1). To analyze how gap junctional coupling can affect the operation of circuits involving both electrical and chemical synapses, we measured the PD to LP neuron synaptic potential and expanded our standard model to include these graded inhibitory synapses (see Methods). Both PD_1 and PD_2 were voltage clamped and held at −60 mV while the LP neuron was recorded in current clamp. Figure 7A (inset) shows the IPSP elicited in the LP neuron when either PD_1 (1VC) or both PD_1 and PD_2

(2VC) were stepped to −20 mV. The larger IPSP amplitude evoked when the two PD neurons were depolarized simultaneously (and consequently uncoupled) is the result of transmitter release from both neurons compared to when a single PD neuron was depolarized. Note that the IPSP was not twice as large in 2VC compared to 1VC indicating that, when only PD_1 was voltage clamped, there was transmitter release from PD_2 as well.

We characterized the voltage-dependence of synaptic release by measuring the amplitude of the IPSP using the 1VC and 2VC voltage clamp protocols with a series of 500 msec depolarizing presynaptic voltage steps of varying amplitudes. The I/O curves for 1VC (coupled, open symbols) and 2VC (uncoupled, filled symbols) are shown in Figure 7A. The IPSPs elicited increased in magnitude as a function of the presynaptic voltage, characteristic of graded synaptic release. When the two PD neurons were uncoupled by using the 2VC protocol, the IPSP amplitudes were significantly larger than for 1VC at all presynaptic membrane potentials (two-way ANOVA, $P = 0.0493$, N = 11). The model of graded synaptic release from the PD to LP neuron closely matched the experimentally observed voltage dependence and captured the difference between voltage clamping one or both PD neurons. Unlike the measurements of the ionic currents, in which uncoupling the two neurons (2VC) led to a reduced total current, the 2VC protocol produced a larger synaptic response in the LP neuron than the 1VC protocol. This difference is due to the fact that, because of the uncoupling that results from the 2VC protocol, the intrinsic currents are measured from a single neuron whereas the synaptic response is due to release from both clamped (but uncoupled) neurons.

Gap junction effects on synaptic transmission

In order to analyze the effects of gap junction coupling on the behavior of a network that includes chemical synapses, we used our model to identify the influence of the relative positions of the gap junction and the chemical synapse on synaptic release. Figure 8 shows the effect of the position of the gap junction and of the chemical synapse along the neuritic cable on synaptic efficacy. Three positions of the gap junction (0, 500 and 1000 μm) were examined along a 1000 μm cable, with 0 indicating the position of the soma. For each gap junction position, the position of the synapse was varied from 0 to 1000 μm along the length of the cable, the soma of neuron 1 or both neurons 1 and 2 of the model was voltage clamped with a voltage pulse from −60 to −20 mV and the postsynaptic potential was measured (neuron 3). Consistent with the observations shown in Figure 7, the 2VC protocol produced a larger IPSP than the 1VC protocol for any position of the chemical synapse (Fig. 8A). This was the result of a better voltage control of the entire second neuron as shown in Figure 8B where we compare the voltage values along both neurites between 1VC and 2VC. In addition to producing better voltage control of neuron 2, the 2VC protocol effectively uncoupled both synapses thus making the IPSP completely independent of the position (and conductance, not shown) of the gap junction. Consequently, the 2VC curve was identical for all gap junction positions (Fig. 8A, black curve). Furthermore, Figure 8A shows that moving the gap junction closer to the site of voltage clamp (i.e. the soma) increased the IPSP amplitude with the 1VC protocol. This was a consequence of less attenuation of the voltage along both neurites as the gap junction was moved closer to the soma (Fig. 8B, compare voltage values along both neurites in the 1VC cases, gap junction position indicated in each schematic

diagram). Notice also that when the gap junction is at an intermediate position between the ends (here at 500 μm), there is a slight kink (discontinuity of the first derivative) in the IPSP amplitude curve at the value for which the position of the chemical synapse matches the position of the gap junction (Fig. 8A, blue trace and black arrowhead). This kink is evident also in the voltage values along the neurite of neuron 1, which show a considerably larger drop between soma and the center of the neurite (500 μm) when the gap junction is placed at the center than when it is placed either at the soma (0 μm) or at the tip (1000 μm) (Fig. 8B, 1VC).

The effects of a gap junction on voltage control along a neurite can be described as the effects of "loading" one neuron with another. Figure 8C shows the effect on a synapse from neuron 1 onto neuron 3 when neuron 1 is "loaded" with a second, identical, neuron via a gap junction at different positions but, in contrast with the case shown in Figures 8A and B, only the voltage clamped neuron 1 made a synapse onto neuron 3 (labeled 1VC$_{½}$; see schematic diagram on the top left of Fig. 8C). We compared this configuration with the case where an isolated neuron 1 made a synapse onto neuron 3 (labeled 1cell; see schematic diagram on the bottom left of Fig. 8C). When the gap junction occurred between the cell bodies (Fig. 8C, red trace), neuron 2 did not affect the membrane potential in neuron 1 due to the fact that the cell body of neuron 1 was voltage clamped and, consequently, the membrane potentials along the neurite of neuron 1 (compare 1VC, gap junction at 0 μm, with 1cell in Fig. 8B) and thus the IPSPs were indistinguishable from the 1cell configuration. (It is important to note that the lack of effect of coupling the cell bodies is due exclusively to the fact that neuron 1 is voltage clamped and thus the second soma does not affect the voltage of neuron 1; in current

clamp the second cell would put a load on neuron 1 and noticeably attenuate voltages along its neurite.) In contrast, when the gap junction occurred at the tip of the neurites, the loading from neuron 2 caused an attenuation of the voltage along the neurite of neuron 1 (Fig. 8C, green trace) compared to the 1cell case (compare 1VC, gap junction at 1000 µm with 1cell in Fig. 8B). Consequently, the IPSP was smaller in amplitude for all positions (except 0 µm) of the chemical synapse compared to the 1cell case. When the gap junction occurred at an intermediate position between the two ends of the neurites (Fig. 8C, blue trace), there was a very strong attenuation of the voltage along the neurite of cell 1 up to the position of the gap junction (Fig. 8B, compare the voltage at 500 µm of 1VC, gap junction at 500 µm with all other cases). At this point there was a sharp kink in the IPSP amplitude curve (Fig. 8C, blue trace and arrowhead). However, the voltage drop from the position of the gap junction (500 µm) to the tip of the neurite (1000 µm) was much smaller than in the other cases. This had the effect that there was a much smaller change in the IPSP amplitude when the position of the chemical synapse was varied between 500 µm and 1000 µm. Interestingly, the largest voltage drop between the soma and the gap junction occurred when the gap junction was near the center of the neurite (compare voltage values of the second diagram in Fig. 8B with those of the first and third diagram). In fact, if neuron 1 and 2 were uniform cables, instead of a sphere and a cable, the strongest attenuation would occur with the gap junction exactly at the center, due to the fact that the input resistance of the second neuron (seen from the position of the gap junction) is lower if the gap junction is in the center of the neurite than at either end.

Interestingly, the kink observed in the 1VC½ case was sharper than in the 1VC configuration where both neuron 1 and neuron 2 made a synapse onto neuron 3. This was

mainly due to the fact that the voltage attenuation along the neurite of neuron 2 was much lower than that of neuron 1 (Fig. 8B, compare the voltages along cable 1 and 2 of 1VC, gap junction at 500 μm) and thus the synaptic transmission from neuron 2 “buffered” the attenuating effect of the gap junction on neuron 1.

DISCUSSION

Electrical coupling via gap junctions is widespread among neurons of the central nervous systems of both vertebrates and invertebrates (Bennett 1997; Dermietzel and Spray 1993). Recently, a number of studies have sought to determine algorithms to minimize errors in the measurement of gap junction conductances (Poznanski 1999; Veenstra 2001). However, the complex morphology of a neuron affects the voltage clamp measurement of ionic currents and the presence of gap junctions in a neuron that is electrically coupled to one or several other neurons can also influence these measurements. To our knowledge, the effect of gap junctions on voltage clamp measurements of ionic currents has not been carefully studied.

We performed voltage-clamp recordings from the two electrically coupled PD neurons of the crustacean stomatogastric ganglion. To estimate the effect of electrical coupling on the measurements of ionic currents and synaptic outputs we used two voltage clamp protocols. In one protocol, we voltage clamped only one PD neuron (1VC) and recorded the second (coupled) PD neuron in current clamp, whereas, in the second protocol, both PD neurons were voltage clamped (2VC), and held at exactly the same membrane potential. Assuming the two PD neurons are anatomically and physiologically identical (Ayali and Harris-Warrick 1999; Eisen and Marder 1984; Hooper 1997; King 1976a, b; Miller and Selverston 1982), the 2VC protocol would functionally uncouple the two PD neurons by eliminating current transfer through the gap junctions. We also used ball-and-stick model neurons with uniform active and passive properties to examine the effect of gap junctions on ionic current measurements in a computational setting.

Gap junction coupling and ionic current measurement errors

Accurate estimation of input resistance, membrane capacitance and voltage-dependent ionic currents requires that these measurements be done in isolated neurons. Otherwise, these measurements would be contaminated by the extra membrane that would effectively be "recruited" through the electrical junctions to the recording configuration. At first glance, our measurements of the voltage-dependent outward currents and the model seem to suggest that the error due to gap junctional coupling is minimal, since there is only a small contribution to the total current by the coupled cell (see Figures 3 and 4B). However, when the current difference due to the gap junctional coupling is expressed as a percentage of the current measured from the uncoupled neuron, it becomes evident that the error is extremely dependent on the size of the measured conductance, with the highest errors obtained for the smallest conductances (Fig. 4A). The largest errors in the biological measurement were at low voltage steps, where the outward current was small. The model confirmed this result when the maximum conductance of the voltage-dependent current was varied: smaller conductances always resulted in larger errors, which can reach values of up to 90% (Fig. 6D). This error is in fact due to the quality of space clamp in the voltage-clamped neuron (1VC protocol), but with the unusual consequence that better space clamp caused a larger error. When the amount of conductance activated is relatively low and therefore the electrotonic size of the voltage clamped neuron is relatively small, the coupled neuron can be strongly influenced from the clamped neuron. As the conductance in neuron 1 is increased, its electrotonic size increases, thus reducing the influence on the coupled

neuron and functionally uncoupling the neurons. As a consequence, the error drops down towards zero. However, the disappearance of the error when conductances are high comes at a price: the distant portions of the neuron contribute little or nothing to the currents measured with the somatic electrodes. This was, for example, apparent in the study of Hartline et al (1993) who showed that there is very little difference in parameter estimation for currents measured in intact PD neurons compared to currents measured in ligated somata of PD neurons.

The small apparent error in estimating voltage-dependent parameters that characterize the outward currents would be considerably larger if the gap junction location was closer to the point of impalement (and current injection). Indeed, as suggested by the model (Fig. 5), the closer the gap junction is to the voltage clamped region (i.e., the soma), the larger is the amount of current recruited from the coupled neuron. Since this current is the result of poorly controlled voltage across the gap junction, paradoxically, for a given gap junctional conductance the error grows larger with improved space clamp (Fig. 5C). Therefore, although errors may not appear large, placing the electrodes in a different position along a neurite that may result in better space clamp may actually further contaminate current measurements by increasing the current flow through gap junctions.

The relatively small errors in our experimental measurements (~23% of the leak conductance —Fig. 2B, and ~10% of the maximal voltage-gated K^+ conductance —Fig. 4B) suggest that the gap junctions between PD neurons in the lobster STG are probably located far away from the soma and close to their dendritic endings, as suggested by the work of Cabirol-Pol et al. (2000). The experimental measurements also show a minimum

error of around 5% (Fig. 4A), which remains approximately constant for all membrane potentials above 0 mV. This is probably an indication that at these membrane potentials, the voltage-dependent current in the PD neurons is maximally activated and that the neuronal input conductance remains constant. From this minimum error we can estimate that the maximum conductance density is close to 5×10^{-3} mS/cm^2 (corresponding to 5% in Fig. 6D), a value very close to the maximal conductance we used in our model.

Errors due to leak subtraction

Our modeling results suggest that between strongly electrically coupled neurons leak subtraction can lead to an additional error than those discussed in the preceding section. This error originates from the subtraction of currents generated during a leak current measurement protocol, when neurons are relatively electrotonically compact, from total current measurements, when neurons are significantly less compact due to the opening of new channels. The difference in actual membrane area under voltage clamp control (higher during the leak current measurement protocol) accounts for an error that can change polarity as a function of the total conductance activated (Fig. 6B, and inset in Fig 6D). This error, however, is relatively small (not exceeding approximately 8%) compared to the errors discussed in the preceding section, and is mainly observed at relatively high leak conductance levels (>0.1 mS/cm^2). However, these high leak conductance levels are often encountered (Buchholtz et al. 1992; Hodgkin and Huxley 1952; Miller et al. 1985; Svirskis et al. 2001) and, in these cases, leak subtraction should be performed with caution. It is important to remember, however, that this leak-

subtraction-associated error occurs when the leak conductance is homogeneously high along the neuronal structure. During an experiment, the leak conductance may increase as a consequence of pharmacological or photoinactivation manipulations. Since this increase in conductance would likely not be localized near the site of impalement, it may lead to errors during the subsequent application of a leak subtraction protocol. In contrast, high measured leak conductances due to microelectrode penetration damage will not have the same effect. Thus, it is useful to determine the leak conductance levels before deciding whether standard leak subtraction protocols should be applied.

Effect of electrical coupling on synaptic properties

Clearly, two presynaptic neurons that are simultaneously active would release more neurotransmitter than a single neuron. However, the efficacy of voltage-dependent (graded) synapses, measured as the amplitude of the postsynaptic potential, depends on many factors. When the two presynaptic neurons are electrically coupled and both synapse onto a third neuron, depolarizing only one of them causes the second neuron to be recruited into releasing neurotransmitter and the combined effect will be larger than if a single, uncoupled, neuron is depolarized, but smaller than if both neurons are depolarized. The release efficacy is nonlinear with respect to the position of the gap junction, with maximal release from the coupled neuron when the gap junction is closest to the soma. Release from both the stimulated and the coupled neurons also depends on the position of the synapse, again with maximal release when the synapse is closest to the soma.

However, if only one of the two coupled neurons is presynaptic, the position of the gap junction plays a more complex role on synaptic release: when the chemical synapse is located between the gap junction and the soma, the farther away the gap junction, the smaller the voltage attenuation and thus the stronger the synaptic release (compare blue and green curves in the range between 0-500 μm in Fig. 8C). Interestingly, in our ball-and-stick model, there is a point along the neurite at which the gap junction has the strongest attenuating effect on the membrane potential, owing to the fact that the input resistance of the second neurite is lower at this point than at either end. An efferent chemical synapse located between the soma and this point will be significantly more attenuated compared to the cases where the gap junction is located either closer to the soma or farther away towards the end of the neurite. A neuron coupled with a gap junction of sufficiently large conductance at this central position of the neurite effectively acts to almost clamp the voltage of its partner for all positions distal from that point. As a consequence of this "voltage clamping" effect, for very distal locations along the neurite, voltage attenuation may turn out to be less significant if the gap junction is located close to the electrotonic center of the neurite than if it is located at the end of it (compare blue and green curves in the range between 700-1000 μm in Fig. 8C).

Gap junctions are know to be more abundant in the developing than in the adult nervous system (Kandler and Katz 1995; Peinado et al. 1993a, b; Vandecasteele et al. 2005) and appear to be critical in the specification of axonal tree structure during development (Wolszon et al. 1994a; Wolszon et al. 1994b). Gap junctional "pruning" has also been suggested to be a potential mechanism for the remodeling of embryonic rhythmic networks into the adult central pattern generating networks (Bem et al. 2002).

Normally, gap junctions in the nervous system seem to occur between the tips of either dendrites or axon terminals (Deboer and Vaney 2005; Garcia-Perez et al. 2004). In spite of the possible effects of interacting chemical and electrical synapses, except for a few estimates (Fukuda and Kosaka 2003; Garcia-Perez et al. 2004), hardly any information exists about their co-localization. Our observations indicate potential interactions of the flowing currents between coupled neurons that may be important for synaptic efficacy. For instance, it seems that in order to preserve a maximal chemical synaptic output while maintaining electrical coupling via gap junctions, it would be best if the chemical synapses are closer to the soma and, in that case, the gap junctions should be distributed either near the tips of the neurites or as close to the soma as possible. These considerations about gap junction and chemical synapse co-localization may be important when using network models involving both types of connections as is the case of the GABAergic interneuron networks of the hippocampus (Fukuda and Kosaka 2000a, b; Skinner et al. 1999; Traub 1995).

Grants

This work was supported by the National Institute of Mental Health Grants MH64711 (J.G.) and MH60605 (F.N.) and the National Science Foundation Grant IBN0090250.

References

Ayali A and Harris-Warrick RM. Monoamine control of the pacemaker kernel and cycle frequency in the lobster pyloric network. *J Neurosci* 19: 6712-6722., 1999.

Bauer R, Lehmann C, Martini J, Eckardt F, and Hoch M. Gap junction channel protein innexin 2 is essential for epithelial morphogenesis in the Drosophila embryo. *Mol Biol Cell* 15: 2992-3004, 2004.

Bem T, Le Feuvre Y, Simmers J, and Meyrand P. Electrical coupling can prevent expression of adult-like properties in an embryonic neural circuit. *J Neurophysiol* 87: 538-547, 2002.

Bennett MV. Gap junctions as electrical synapses. *J Neurocytol* 26: 349-366, 1997.

Bennett MV and Zukin RS. Electrical coupling and neuronal synchronization in the Mammalian brain. *Neuron* 41: 495-511, 2004.

Buchholtz F, Golowasch J, Epstein IR, and Marder E. Mathematical model of an identified stomatogastric ganglion neuron. *J Neurophysiol* 67: 332-340, 1992.

Cabirol-Pol MJ, Mizrahi A, Simmers J, and Meyrand P. Combining laser scanning confocal microscopy and electron microscopy to determine sites of synaptic contact between two identified neurons [In Process Citation]. *J Neurosci Methods* 97: 175-181, 2000.

Dahle J, Angell-Petersen E, Steen HB, and Moan J. Bystander effects in cell death induced by photodynamic treatment UVA radiation and inhibitors of ATP synthesis. *Photochem Photobiol* 73: 378-387, 2001.

Deboer DJ and Vaney DI. Gap-junction communication between subtypes of direction-selective ganglion cells in the developing retina. *J Comp Neurol* 482: 85-93, 2005.

Dermietzel R and Spray DC. Gap junctions in the brain: where, what type, how many and why? *Trends Neurosci* 16: 186-192, 1993.

Edwards DH, Yeh SR, and Krasne FB. Neuronal coincidence detection by voltage-sensitive electrical synapses. *Proc Natl Acad Sci U S A* 95: 7145-7150, 1998.

Eisen JS and Marder E. A mechanism for production of phase shifts in a pattern generator. *J Neurophysiol* 51: 1375-1393, 1984.

Eisen JS and Marder E. Mechanisms underlying pattern generation in lobster stomatogastric ganglion as determined by selective inactivation of identified neurons. III. Synaptic connections of electrically coupled pyloric neurons. *J Neurophysiol* 48: 1392-1415, 1982.

Fukuda T and Kosaka T. The dual network of GABAergic interneurons linked by both chemical and electrical synapses: a possible infrastructure of the cerebral cortex. *Neurosci Res* 38: 123-130, 2000a.

Fukuda T and Kosaka T. Gap junctions linking the dendritic network of GABAergic interneurons in the hippocampus. *J Neurosci* 20: 1519-1528, 2000b.

Fukuda T and Kosaka T. Ultrastructural study of gap junctions between dendrites of parvalbumin-containing GABAergic neurons in various neocortical areas of the adult rat. *Neuroscience* 120: 5-20, 2003.

Garcia-Perez E, Vargas-Caballero M, Velazquez-Ulloa N, Minzoni A, and De-Miguel FF. Synaptic integration in electrically coupled neurons. *Biophys J* 86: 646-655, 2004.

Golowasch J, Goldman MS, Abbott LF, and Marder E. Failure of averaging in the construction of a conductance-based neuron model. *J Neurophysiol* 87: 1129-1131, 2002.

Golowasch J and Marder E. Ionic currents of the lateral pyloric neuron of the stomatogastric ganglion of the crab. *J Neurophysiol* 67: 318-331., 1992.

Graubard K and Hartline DK. Voltage clamp analysis of intact stomatogastric neurons. *Brain Res* 557: 241-254, 1991.

Harris-Warrick RM. *Dynamic biological networks : the stomatogastric nervous system*. Cambridge, Mass.: MIT Press, 1992.

Harris-Warrick RM, Coniglio LM, Barazangi N, Guckenheimer J, and Gueron S. Dopamine modulation of transient potassium current evokes phase shifts in a central pattern generator network. *J Neurosci* 15: 342-358, 1995.

Hartline DK and Castelfranco AM. Simulations of voltage clamping poorly space-clamped voltage-dependent conductances in a uniform cylindrical neurite. *J Comput Neurosci* 14: 253-269, 2003.

Hartline DK, Gassie DV, and Jones BR. Effects of soma isolation on outward currents measured under voltage clamp in spiny lobster stomatogastric motor neurons. *J Neurophysiol* 69: 2056-2071, 1993.

Hodgkin AL and Huxley AF. A quantitative description of membrane current and its application to conduction and excitation in nerve. *J Physiol* 117: 500-544, 1952.

Hooper SL. Phase maintenance in the pyloric pattern of the lobster (Panulirus interruptus) stomatogastric ganglion. *J Comput Neurosci* 4: 191-205, 1997.

Johnson BR, Kloppenburg P, and Harris-Warrick RM. Dopamine modulation of calcium currents in pyloric neurons of the lobster stomatogastric ganglion. *J Neurophysiol* 90: 631-643, 2003.

Johnston D and Wu SM-s. *Foundations of cellular neurophysiology*. Cambridge, Mass.: MIT Press, 1995.

Kam Y, Kim DY, Koo SK, and Joe CO. Transfer of second messengers through gap junction connexin 43 channels reconstituted in liposomes. *Biochim Biophys Acta* 1372: 384-388, 1998.

Kandler K and Katz LC. Coordination of neuronal activity in developing visual cortex by gap junction-mediated biochemical communication. *J Neurosci* 18: 1419-1427, 1998.

Kandler K and Katz LC. Neuronal coupling and uncoupling in the developing nervous system. *Curr Opin Neurobiol* 5: 98-105, 1995.

King DG. Organization of crustacean neuropil. I. Patterns of synaptic connections in lobster stomatogastric ganglion. *J Neurocytol* 5: 207-237, 1976a.

King DG. Organization of crustacean neuropil. II. Distribution of synaptic contacts on identified motor neurons in lobster stomatogastric ganglion. *J Neurocytol* 5: 239-266, 1976b.

Komendantov AO and Canavier CC. Electrical coupling between model midbrain dopamine neurons: effects on firing pattern and synchrony. *J Neurophysiol* 87: 1526-1541, 2002.

Mesnil M. Connexins and cancer. *Biol Cell* 94: 493-500, 2002.

Miller JP, Rall W, and Rinzel J. Synaptic amplification by active membrane in dendritic spines. *Brain Res* 325: 325-330, 1985.

Miller JP and Selverston A. Rapid killing of single neurons by irradiation of intracellularly injected dye. *Science* 206: 702-704, 1979.

Miller JP and Selverston AI. Mechanisms underlying pattern generation in lobster stomatogastric ganglion as determined by selective inactivation of identified neurons. II. Oscillatory properties of pyloric neurons. *J Neurophysiol* 48: 1378-1391, 1982.

Moore H and Grace AA. A role for electrotonic coupling in the striatum in the expression of dopamine receptor-mediated stereotypies. *Neuropsychopharmacology* 27: 980-992, 2002.

Peinado A, Yuste R, and Katz LC. Extensive dye coupling between rat neocortical neurons during the period of circuit formation. *Neuron* 10: 103-114, 1993a.

Peinado A, Yuste R, and Katz LC. Gap junctional communication and the development of local circuits in neocortex. *Cereb Cortex* 3: 488-498, 1993b.

Perez-Velazquez JL, Valiante TA, and Carlen PL. Modulation of gap junctional mechanisms during calcium-free induced field burst activity: a possible role for electrotonic coupling in epileptogenesis. *J Neurosci* 14: 4308-4317, 1994.

Pfeuty B, Mato G, Golomb D, and Hansel D. Electrical synapses and synchrony: the role of intrinsic currents. *J Neurosci* 23: 6280-6294, 2003.

Poznanski RR. Electrophysiology of a leaky cable model for coupled neurons. *J Austral Math Soc Ser B* 40: 59-71, 1999.

Prinz AA, Bucher D, and Marder E. Similar network activity from disparate circuit parameters. *Nat Neurosci*, 2004.

Rall W, Segev I, Rinzel J, and Shepherd GM. *The theoretical foundation of dendritic function : selected papers of Wilfrid Rall with commentaries*. Cambridge, Mass.: MIT Press, 1995.

Raper JA. Nonimpulse-mediated synaptic transmission during the generation of a cyclic motor program. *Science* 205: 304-306, 1979.

Rorig B, Klausa G, and Sutor B. Intracellular acidification reduced gap junction coupling between immature rat neocortical pyramidal neurones. *J Physiol* 490 (Pt 1): 31-49, 1996.

Rose CR and Konnerth A. Exciting glial oscillations. *Nat Neurosci* 4: 773-774, 2001.

Saez JC, Connor JA, Spray DC, and Bennett MV. Hepatocyte gap junctions are permeable to the second messenger, inositol 1,4,5-trisphosphate, and to calcium ions. *Proc Natl Acad Sci U S A* 86: 2708-2712, 1989.

Saint-Amant L and Drapeau P. Synchronization of an embryonic network of identified spinal interneurons solely by electrical coupling. *Neuron* 31: 1035-1046, 2001.

Selverston AI, Russell DF, and Miller JP. The stomatogastric nervous system: structure and function of a small neural network. *Prog Neurobiol* 7: 215-290, 1976.

Skinner FK, Zhang L, Velazquez JL, and Carlen PL. Bursting in inhibitory interneuronal networks: A role for gap-junctional coupling. *J Neurophysiol* 81: 1274-1283, 1999.

Sullivan R, Huang GY, Meyer RA, Wessels A, Linask KK, and Lo CW. Heart malformations in transgenic mice exhibiting dominant negative inhibition of gap junctional communication in neural crest cells. *Dev Biol* 204: 224-234, 1998.

Svirskis G, Gutman A, and Hounsgaard J. Electrotonic structure of motoneurons in the spinal cord of the turtle: inferences for the mechanisms of bistability. *J Neurophysiol* 85: 391-398, 2001.

Traub RD. Model of synchronized population bursts in electrically coupled interneurons containing active dendritic conductances. *J Comput Neurosci* 2: 283-289, 1995.

Traub RD, Schmitz D, Jefferys JG, and Draguhn A. High-frequency population oscillations are predicted to occur in hippocampal pyramidal neuronal networks interconnected by axoaxonal gap junctions. *Neuroscience* 92: 407-426, 1999.

Tresch MC and Kiehn O. Motor coordination without action potentials in the mammalian spinal cord. *Nat Neurosci* 3: 593-599, 2000.

Trosko JE and Chang CC. Mechanism of up-regulated gap junctional intercellular communication during chemoprevention and chemotherapy of cancer. *Mutat Res* 480-481: 219-229, 2001.

Vandecasteele M, Glowinski J, and Venance L. Electrical Synapses between Dopaminergic Neurons of the Substantia Nigra Pars Compacta. *J Neurosci* 25: 291-298, 2005.

Veenstra RD. Voltage clamp limitations of dual whole-cell gap junction current and voltage recordings. I. Conductance measurements. *Biophys J* 80: 2231-2247, 2001.

Whittington MA and Traub RD. Interneuron diversity series: inhibitory interneurons and network oscillations in vitro. *Trends Neurosci* 26: 676-682, 2003.

Wolszon LR, Gao WQ, Passani MB, and Macagno ER. Growth cone "collapse" in vivo: are inhibitory interactions mediated by gap junctions? *J Neurosci* 14: 999-1010, 1994a.

Wolszon LR, Rehder V, Kater SB, and Macagno ER. Calcium wave fronts that cross gap junctions may signal neuronal death during development. *J Neurosci* 14: 3437-3448, 1994b.

Figure Legends

Figure 1. *Experimental recording configuration*. **A**. Intracellular recordings of the PD and LP neurons in normal saline. The minimum membrane potentials during the oscillations were −50 mV for PD_1, −54mV for PD_2 and −58mV for LP. *Inset.* Schematic diagram showing the experimental setup and network connectivity diagram. For simplicity we assumed the electrical and chemical synapses to be all located at the end of long neurites. This diagram also depicts the model network, in which the neurites were modeled as a homogeneous cables divided into several compartments. **B**. In the presence of 10^{-7} M TTX, both PD neurons were voltage-clamped and held at V_{hold}= −40 mV (top panel). The middle traces show I_{PD_1} and I_{PD_2} in response to steps to −50 mV (thin traces) and 0 mV (thick traces) applied simultaneously to both PD neurons. V_{LP} was monitored in current clamp (bottom panel). Thick trace corresponds to the synaptic response to PD depolarization, thin traces to PD hyperpolarization.

Figure 2. *Gap junctional coupling affects measurements of passive currents*. **A**. PD_1 was voltage clamped at V_{hold} = −40 mV and a 10 mV hyperpolarizing step was applied. The passive current elicited in PD_1 was recorded, I_{PD_1} (bottom panel, 1VC, thick trace) while PD_2 was recorded in current clamp (middle panel, 1VC, thick trace). The PD_2 resting potential was −45 mV. Both PD neurons were then voltage clamped simultaneously (V_{hold} = −40 mV), the hyperpolarizing step was repeated and the leak currents elicited in PD_1 (bottom panel) as well as the voltage in PD_2 (middle panel) were recorded (2VC, thin traces). **B**. Average leak conductance (±SD) measured in PD_1 for 1VC (0.238 ± 0.144 μS) and for 2VC (0.193 ± 0.109 μS; Student's *t*-test, P = 0.00846; N = 12).

Figure 3. *Effect of gap junctional coupling on voltage-gated currents*. **A**. Total current measured in the PD_1 neuron when depolarized to levels ranging from −30 mV to +20 mV (top panel). Thick traces correspond to when only PD_1 was clamped (1VC) and thin traces when both PD neurons were clamped to identical voltages (2VC), and thus were electrically uncoupled. V_{hold} = −40 mV. Top panel of current traces corresponds to the biological neurons and the bottom panel to the conductance-based model. **B**. *I-V* curves obtained from the data in A. Currents were measured at their peak (between 50-100 ms after pulse onset) and steady-state (at the end of the 2 s pulse). In both cases, currents were significantly larger when only one PD neuron was voltage clamped (1VC, solid symbols) than when both PD neurons were clamped and thus uncoupled (2VC, open symbols). The bottom panel shows the equivalent measurements in the model.

Figure 4. *Error estimates of voltage-dependent current measurements in coupled neurons*. **A**. Error in the measurement of leak-subtracted currents measured at steady state expressed as the percent difference between currents in the coupled (1VC) and uncoupled (2VC) neurons relative to the measurements in one uncoupled (2VC) neuron, calculated from the leak-subtracted average values of the same data as in Figure 3, Biological (N = 12). **B**. Leak-subtracted steady state mean conductances (current divided by driving force) measured in 1VC and 2VC and the corresponding fits with a the Boltzman function: $Gmax / (1+e^{-k[V+V½]})$. Best fit parameter values are for 1VC: Gmax = 1.79 µS, V½ = −0.4 mV, k = 0.100 mV; and for 2VC: Gmax = 1.63 µS, V½ = −0.6 mV, k = 0.107 mV). As in A, the data used are the same as those shown in Figure 3, Biological.

Figure 5. Effect of the position of the gap junction on current measurements. **A**. Diagrams of the recording and coupling configurations of two identical model neurons of

fixed length 1000 μm (i-iii) with the gap junction located at 100 μm, 500 μm or 1000 μm distance from the soma or when the model neuron length was varied (1000, 500 or 100 μm, iii-v) with the gap junction always located at the end of the neurites. Below the diagrams are the total currents recorded when only one (red, coupled) or both (black, uncoupled) PD model neurons were clamped (voltage step from −40mV to +20mV). Dashed line is at the peak current of iii, shown for comparison of total currents in the different conditions. **B**. Total steady-state currents measured as a function of the position of the gap junction along the cable. Open symbols correspond to variation of the gap junction along the 1000 μm long cable. Solid symbols correspond to the case when the gap junction occurred at the end of cables of varying length. **C**. Normalized current difference from data in panel B showing the percentage that the 1VC current measured was larger than the 2VC current.

Figure 6. *Effect of modifying leak and K^+ conductances on current measurements of coupled model neurons*. All current measurements were made in the *standard model* with a test pulse from −40 to +20 mV. **A**. Total currents measured when both model neurons were coupled (1VC) or uncoupled (2VC) as the leak conductance was varied. *Inset*: Magnification of the shaded region to highlight small but significant differences between 1VC and 2VC. **B**. The current difference between 1VC and 2VC as a percentage of the current measured in 2VC shown as a function of the leak conductance. Red circles show the percent difference when both 1VC and 2VC currents were leak subtracted before normalization. **C**. Total currents measured at steady state as the maximal conductance of the K^+ current was varied. Values of GKmax shown are $\bar{g}_{KS}$, but $\bar{g}_{KF}$ was also varied by the same proportion as in the standard model. *Inset*: Magnification of the

shaded region to highlight small but significant differences between 1VC and 2VC. Legend is the same as A. This inset shows that the 1VC differs from the 2VC measured current mainly in a conductance interval around and below that of the standard model (5 mS/cm^2). **D**. The current difference between the 1VC and 2VC conditions as a percentage of the current measured in 2VC shown as a function of GKmax. *Inset*: Magnification of region between 5 and 1000 mS/cm^2. Legend is the same as in B.

Figure 7. *Graded inhibitory postsynaptic potentials and electrical coupling*. **A**. One (1VC) or both (2VC) PD neurons were voltage clamped ($V_{hold} = -60$ mV) and the peak IPSP evoked in the LP neuron was recorded in current clamp (resting potential −50 mV) in response to 500 ms depolarizing voltage steps to various levels applied to the PD neuron(s). For all values of V_{PD} (−50 to −10 mV), synaptic potentials were larger (more negative) when both PD neurons, rather than only one PD neuron, were voltage clamped. The inset illustrates one such step to −20 mV. **B**. Same experimental procedure applied to the standard model of synaptic release described in Methods.

Figure 8. *Effect of position of the chemical inhibitory synapse relative to the position of the gap junction*. Three gap junction positions were used (0, 500 and 1000 μm; marked with colored dots on the diagrams on the left of A and C). For each gap junction position, the position of the chemical synapse was varied along the entire cable. Positions are relative to the soma, which is at 0 μm. All measurements were made with a voltage pulse from −60mV to −20mV. **A**. Synaptic potentials measured as the difference between baseline and peak (see inset in Fig. 7A). Either only one (colored curves, 1VC) or both (black curve, 2VC) neurons were voltage clamped. Arrowhead points to a kink in the trace at the position of the gap junction (here, at 500 μm). When both neurons were

voltage clamped, the position of the gap junction was irrelevant and the traces were perfectly superimposed (black curve, 2VC). Diagrams on the left show schematic representations of the positions of the gap junction and the chemical synapses as well as the recording configurations. The arrows in the diagrams indicate varying positions of the gap junction and of the chemical synapse. **B**. Diagrams of recording configurations showing three different gap junction positions and the membrane potential values (in mV) recorded at the same 3 positions in each neurite, in 1VC (left three diagrams) and 2VC (right diagram, gap junctions dimmed). Notice that in 2VC, the voltages along both neurites were the same as for 1VC when the soma of neuron 1 was clamped and the gap junction position was 0 μm. **C**. Recording of peak synaptic potential in two different geometric and recording configurations as shown in the diagrams to the left. In both, the chemical synapse originated only from neuron 1. In the "1VC½" configuration, neuron 2 added a "load" onto neuron 1 via a gap junction at different positions. In the "1cell" configuration, the two cells were clamped to the same voltages and were thus uncoupled. Arrowhead points to a kink in the trace at a position where both the gap junction and the chemical synapse coincide (500μm). Voltages along the neurite of neuron 1 in the 1VC½ configuration are identical to those in 1VC shown in B. Voltages in the "1cell" configuration are identical to those of 2VC shown in B.

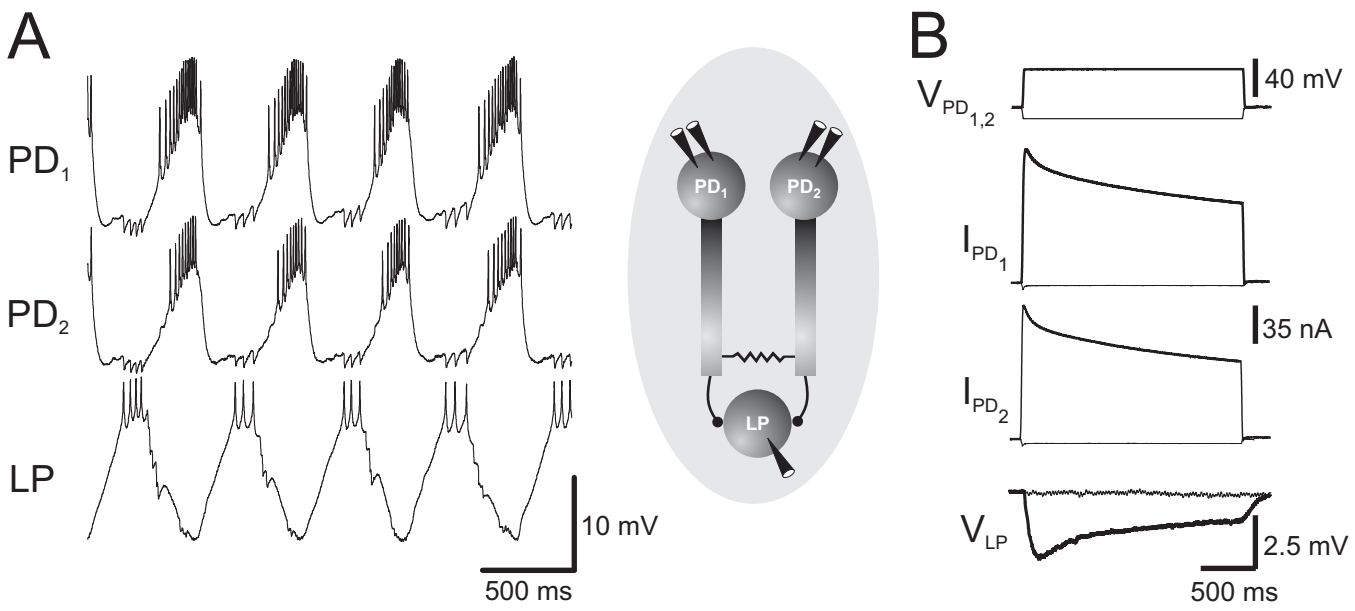

Figure 1
Rabbah, Golowasch & Nadim

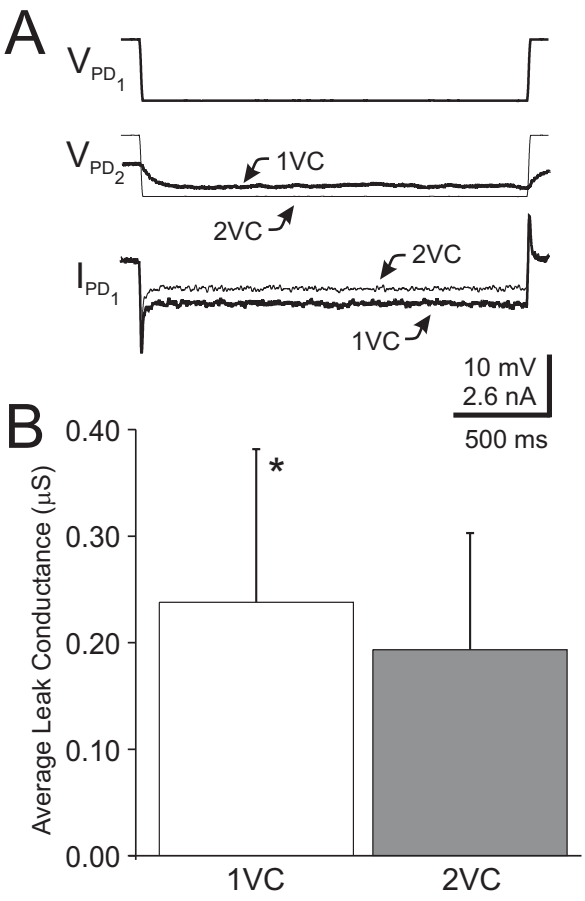

Figure 2
Rabbah, Golowasch & Nadim

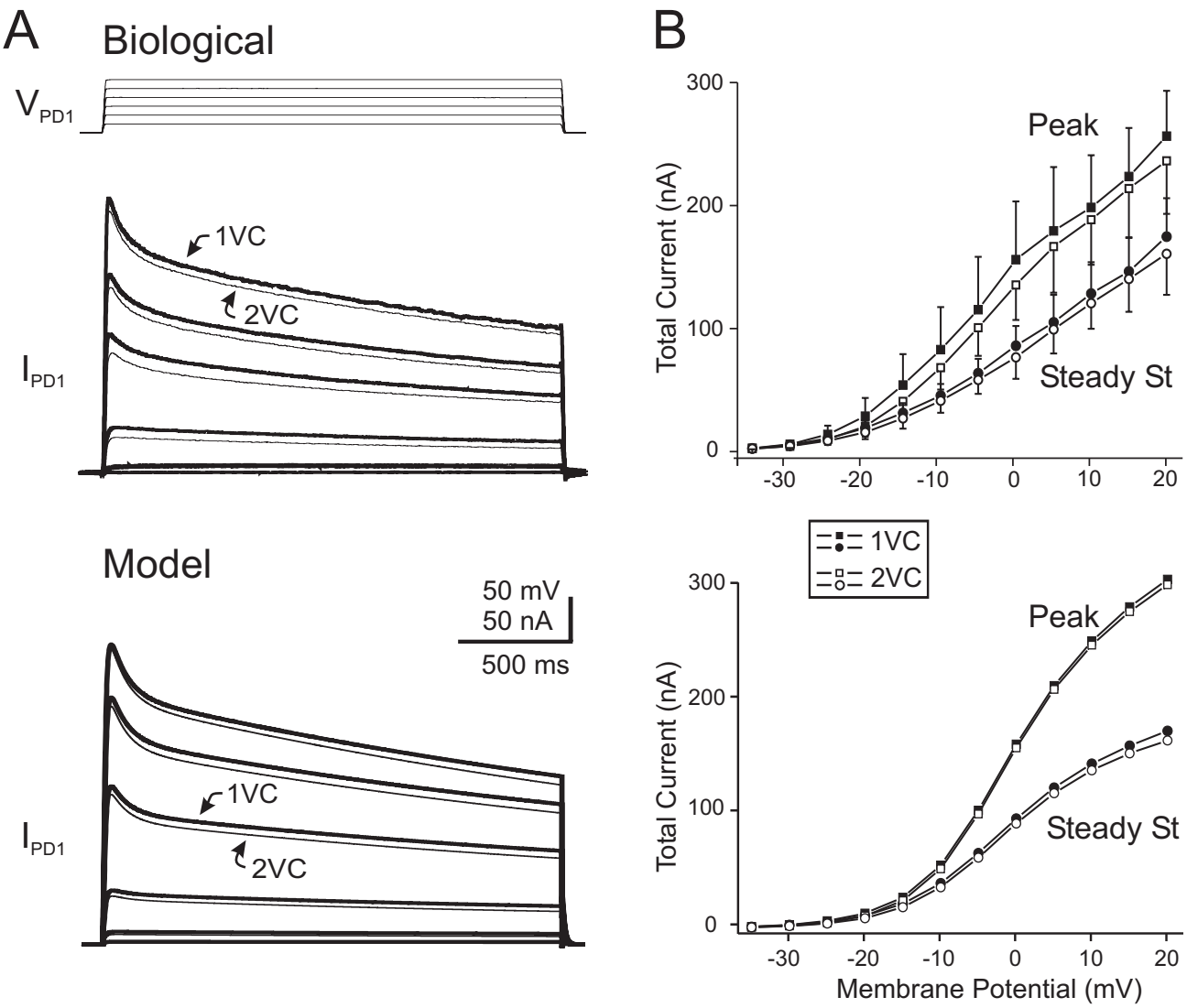

Figure 3
Rabbah, Golowasch & Nadim

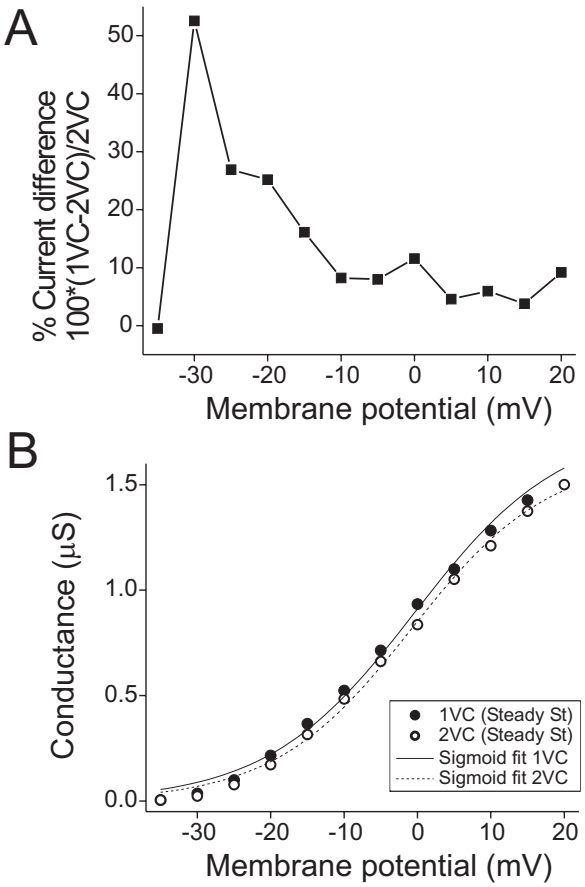

Figure 4
Rabbah, Golowasch & Nadim

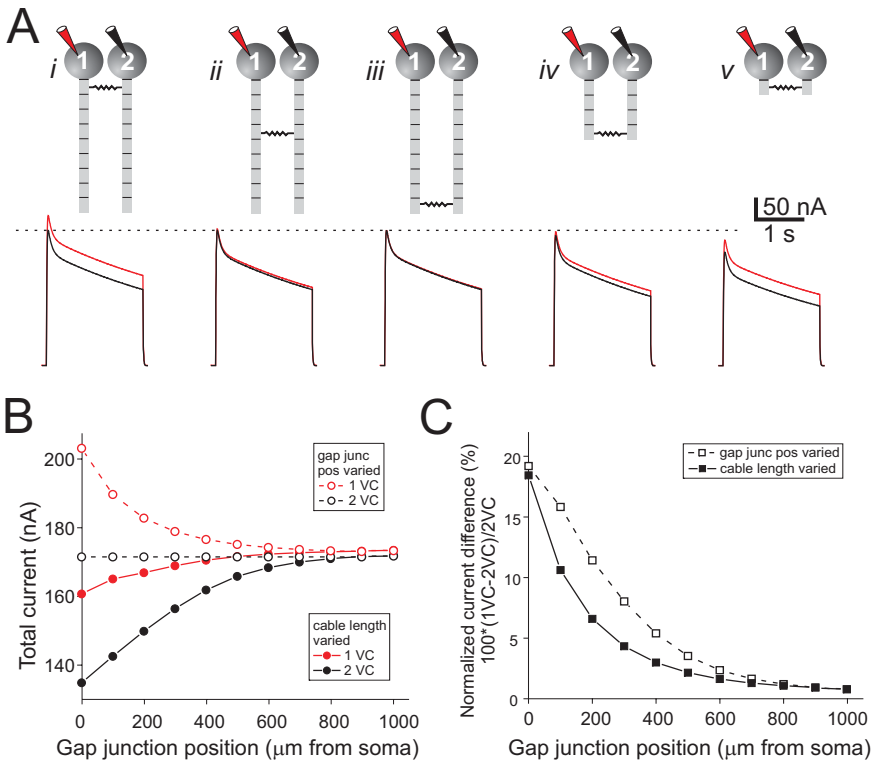

Figure 5
Rabbah, Golowasch & Nadim

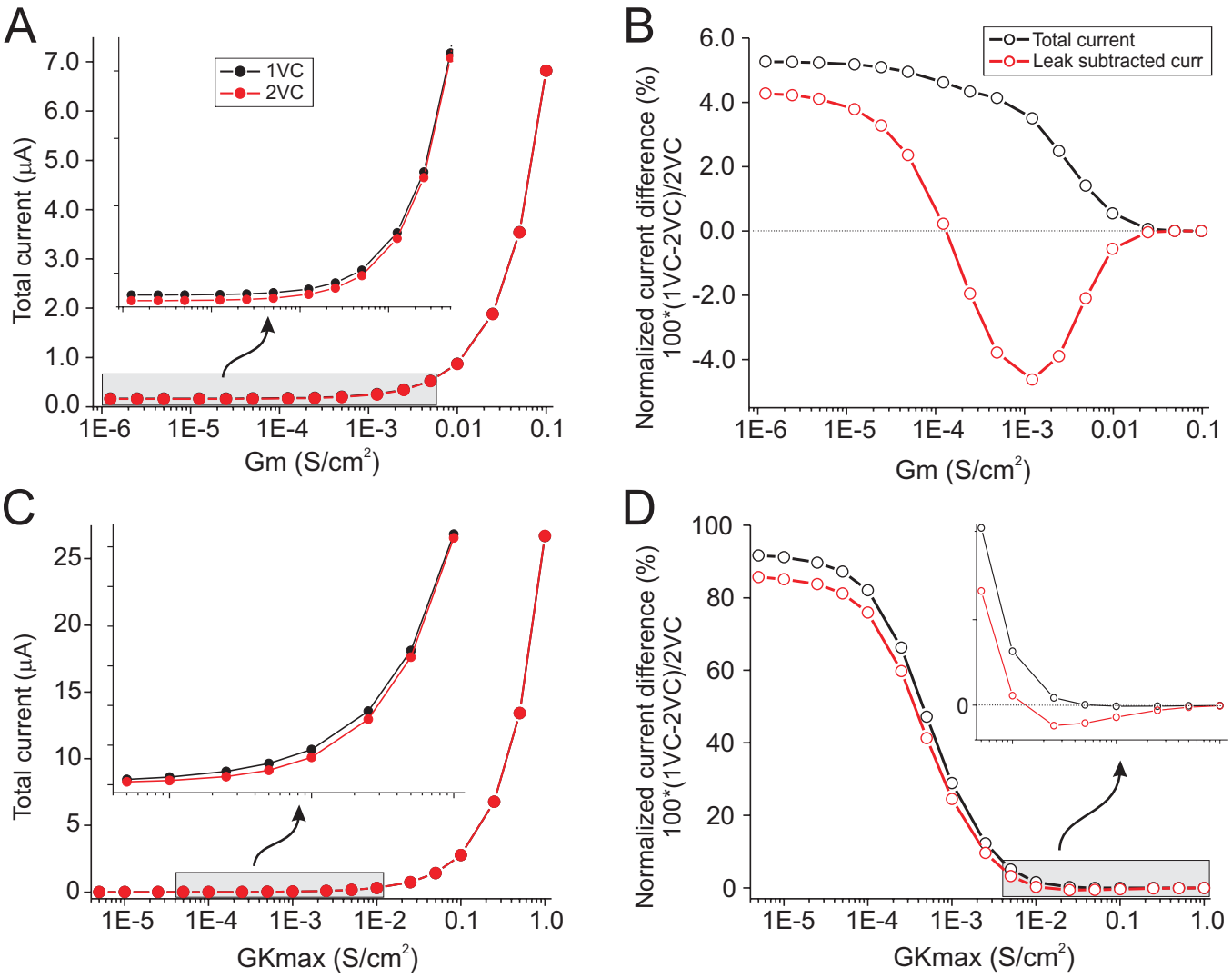

Figure 6
Rabbah, Golowasch & Nadim

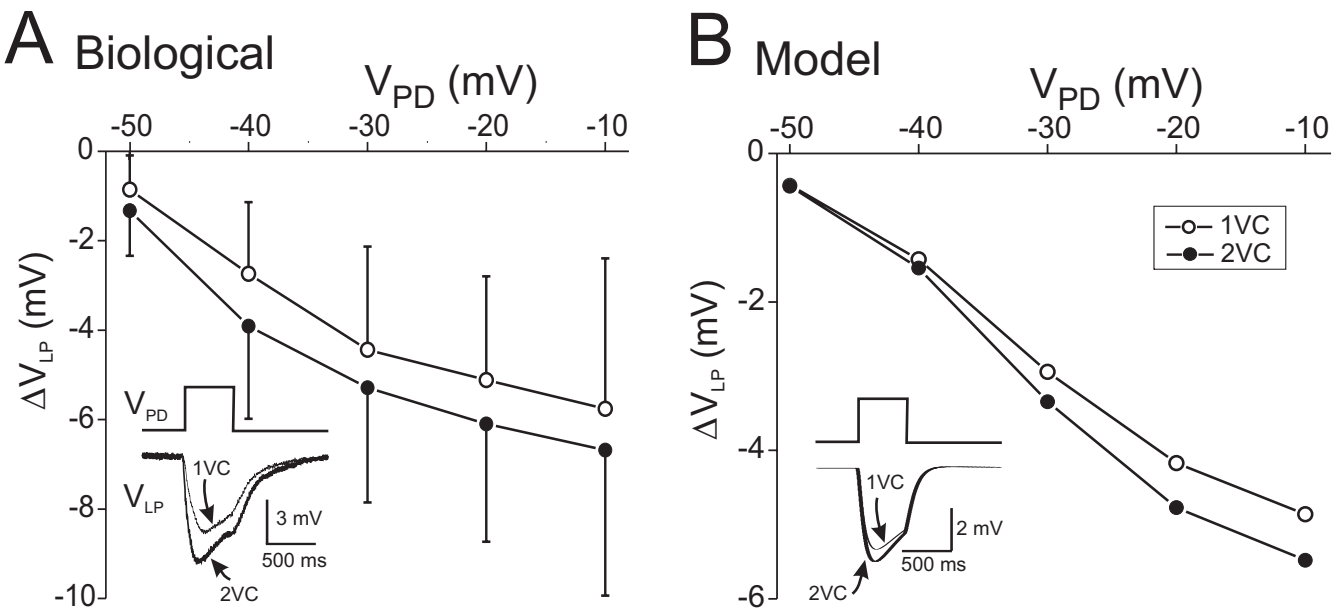

Figure 7
Rabbah, Golowasch & Nadim

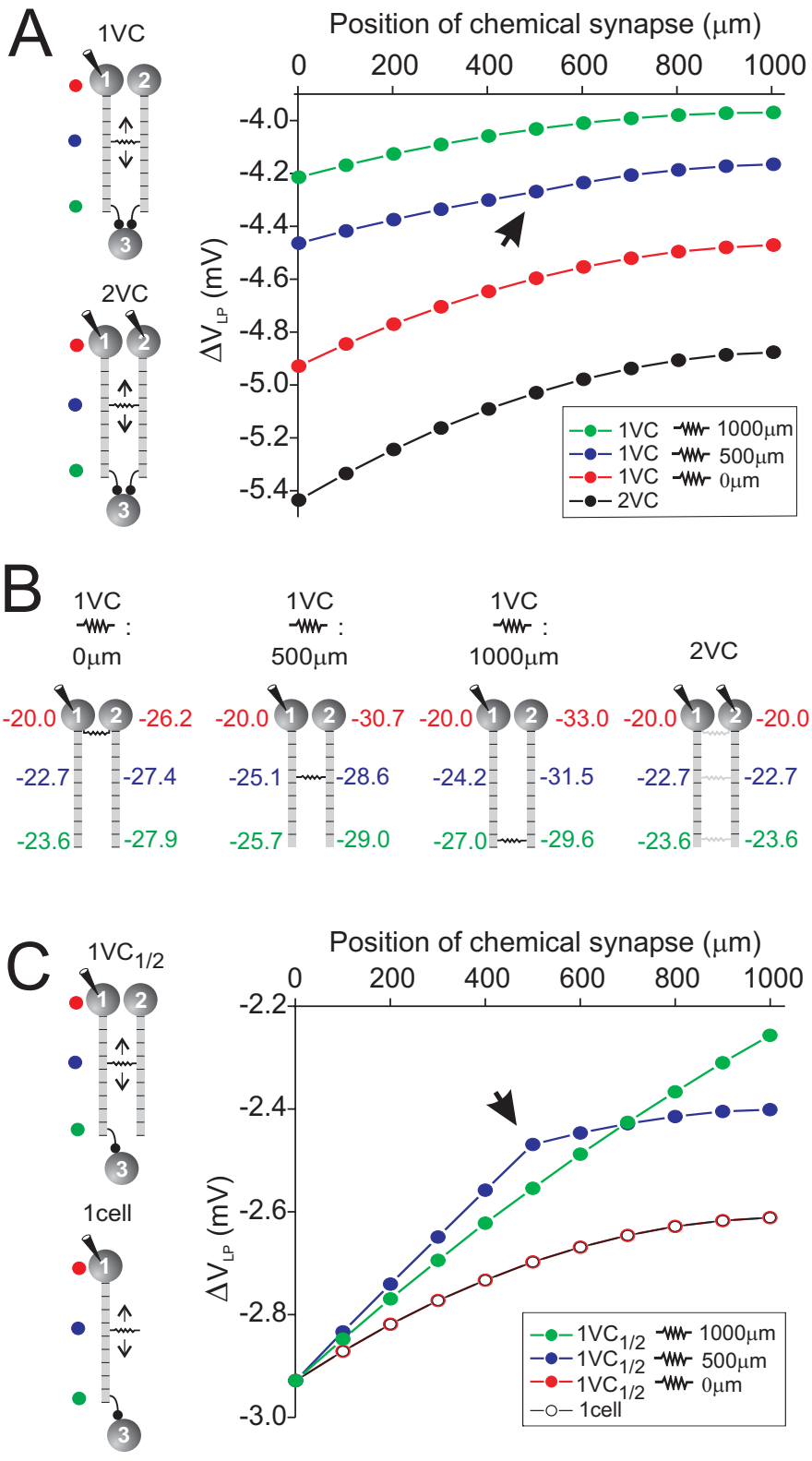

Figure 8
Rabbah, Golowasch & Nadim